

# Flow-Based Synthesis of Gold-Coated Magnetic Nanoparticles for Magnetoplasmonic Sensing Applications

Milad Mehdipour, Lucy Gloag,\* Daniel Hagness, Jiaxin Lian, Md Saiful Alam, Xueqian Chen, Richard D. Tilley,\* and John Justin Gooding\*

Gold-coated magnetic nanoparticles are key materials for the fast separation and ultrasensitive detection of analytes in magnetoplasmonic sensors. However, the synthesis of gold-coated magnetic nanoparticles typically requires small-scale, colloidal methods over hours or days and often results in incomplete shells with variable optical properties. A robust, rapid, and scalable synthesis method is still needed to reliably form a complete gold nanoshell around magnetic nanoparticles. Herein, a new methodology for the synthesis of gold-coated magnetic nanoparticles via a flow-based manufacturing system that can easily be scaled up is presented. The developed method first produces gold-seeded silica coated magnetic nanoparticles and then a complete, tunable gold shell with relatively uniform size and shape. The flow-based method can be performed in a total time of less than 2 min, enabling rapid and complete gold coating. The particles show both excellent magnetic and plasmonic properties, which facilitates application as biosensing agents in dark-field microscopy and surface-enhanced Raman scattering.

plasmon resonance, and fast magnetic response in a single system, which opens numerous possibilities for facilitating diagnostics and treatment of diseases.<sup>[1–6]</sup> For magnetoplasmonic sensing, the magnetic nanoparticles need to be completely coated with a gold shell. Effective coating ensures that the magnetic nanoparticles are not exposed to air or biological media, which can cause particle degradation and lower the magnetic susceptibility.<sup>[3,6–9]</sup> A complete shell also produces uniform absorbance, which is important for detecting plasmonic shifts due to analyte absorption.<sup>[10–12]</sup>

The coating of magnetic nanoparticles with gold is synthetically challenging. Stepwise colloidal synthesis over hours or days has been the most effective method to achieve gold-coated magnetic nano-

## 1. Introduction


Gold-coated magnetic nanoparticles are attracting interest for biosensing due to their dual magnetoplasmonic properties. They combine highly desirable properties such as conductivity, bioconjugation capability, chemical stability, localized surface

particles, as this approach enables control over nucleation and growth stages separately to achieve coating across the entire sample.<sup>[11–16]</sup> A robust, scalable, and automated method is needed to rapidly coat larger sample sizes. Flow-based synthesis is promising method to achieve scalable and precise nanomaterial production. Flow reactors can achieve superior reagents mixing and homogeneity, effective heat, and mass transfer which creates controlled growth of uniform products in seconds to minutes timescales.<sup>[17–21]</sup>

Herein, we present a facile flow-based system for the seeding of silica coated magnetic nanoparticles and growth of complete gold shells that can be performed within 2 min. The strategy uses syringe pumps and a Y-shaped piece with channels for intimate mixing of reagents. We show that the flow-based method enables control over the thickness of the resulting gold shell, which creates tunable optical properties without significant reduction in the magnetic performance. Finally, we demonstrate that the magnetoplasmonic particles produced from this method can be used to bind to biomolecules and act as biosensing agents for surface-enhanced Raman spectroscopy (SERS).

M. Mehdipour, L. Gloag, D. Hagness, J. Lian, M. S. Alam, X. Chen, R. D. Tilley, J. J. Gooding  
School of Chemistry  
The University of New South Wales  
Sydney, New South Wales 2052, Australia  
E-mail: l.gloag@unsw.edu.au; r.tilley@unsw.edu.au; justin.gooding@unsw.edu.au

R. D. Tilley  
Electron Microscope Unit  
Mark Wainwright Analytical Centre  
The University of New South Wales  
Sydney, New South Wales 2052, Australia  
R. D. Tilley, J. J. Gooding  
Australian Centre for NanoMedicine  
The University of New South Wales  
Sydney, New South Wales 2052, Australia

 The ORCID identification number(s) for the author(s) of this article can be found under <https://doi.org/10.1002/ppsc.202200051>.

© 2022 The Authors. Particle & Particle Systems Characterization published by Wiley-VCH GmbH. This is an open access article under the terms of the Creative Commons Attribution License, which permits use, distribution and reproduction in any medium, provided the original work is properly cited.

DOI: 10.1002/ppsc.202200051

## 2. Results and Discussion

### 2.1. Gold-Coating Method

A schematic of this method is shown in **Figure 1**, and Y-shaped pieces are illustrated in Figure S1 of the Supporting Information. The two Y-shaped tube connectors combine the flows

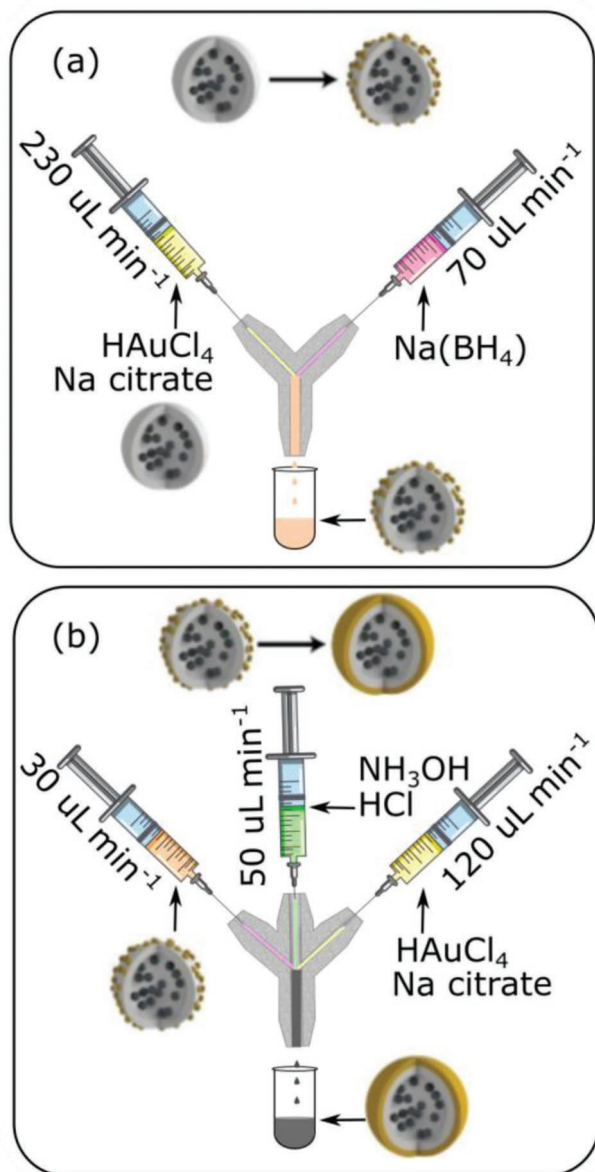


**Figure 1.** Schematic of a) seeding manufacturing method using a two-channel syringe set-up and b) gold nanoshell manufacturing method using a three-channel syringe set-up.

from each syringe to create an intimate mixture of reactants. The simple design of the system developed here not only solves the problem of clogging but offers a disposable system capable of coating the magnetic nanoparticles with a gold shell in a scalable fashion.

The first system (Figure 1a) attaches small gold nanoparticles to the surface of silica. Silica-coated magnetic nanoparticles (Figure S2, Supporting Information) were loaded into Syringe 1 with gold chloride and sodium citrate aqueous solution, and an aqueous solution of sodium borohydride (0.01 M) was loaded into Syringe 2. Optimal mixing was achieved with a flow rate of  $230 \mu\text{L min}^{-1}$  for Syringe 1, and  $70 \mu\text{L min}^{-1}$  for Syringe 2. During the reaction, gold seeds were synthesized and attached to the silica surface.

Reducing the gold chloride with a strong reducing agent like sodium borohydride in the presence of sodium citrate produces small gold nanoparticles with a negative charge on the surface.<sup>[22]</sup> The surface of the silica-coated magnetic nanoparticles is fully covered with  $\approx 3$  nm gold nanoparticles (visible as black dots, Figure S3, Supporting Information). A dense seeding of the surface with ultrasmall gold nanoparticles is the key to the formation of a complete gold shell as these small gold nanoparticles act as catalytic sites for gold nanoshell formation.<sup>[11,15,23,24]</sup>

The second system (Figure 1b) grows the gold shell around pre-gold seeded silica-coated magnetic nanoparticles. Gold seeded silica-coated magnetic nanoparticles were loaded inside Syringe 3, an aqueous solution of gold chloride and sodium citrate was loaded in Syringe 4 and, an aqueous solution of hydroxylamine hydrochloride reducing agent was in Syringe 5. To achieve uniform growth of the gold shell, flow rates of  $30 \mu\text{L min}^{-1}$  for Syringe 3,  $120 \mu\text{L min}^{-1}$  for Syringe 4 and  $50 \mu\text{L min}^{-1}$  for Syringe 5 were found to be optimal. A drop of the reaction solution was deposited onto a transmission electron microscopy (TEM) grid to ensure that the pre-gold seeded silica-coated magnetic nanoparticles are fully gold-coated before leaving the channel (Figure S4, Supporting Information). For both gold seeding and coating steps, over 95% nanoparticles had gold deposited. After purification to remove excess reagents and aggregates, yields of 40–60% were achieved.

The thickness of the gold shell can be tuned by adjusting the concentration of pre-gold seeded silica-coated magnetic nanoparticles in Syringe 3 and keeping the other concentrations constant. Below  $2 \times 10^{-9}$  M, the gold-coating was incomplete and results in aggregation of nanoparticles (Figure 2a). The low concentration of pre-gold seeded silica-coated magnetic

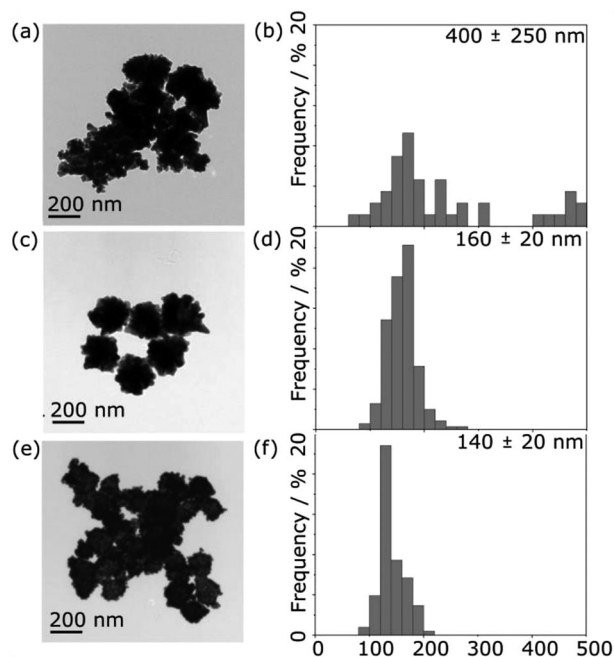


**Figure 2.** TEM images and histograms of the size distributions of gold-coated magnetic nanoparticles prepared with different initial pre-gold seeded silica-coated magnetic nanoparticles concentration. a,b)  $2 \times 10^{-9}$  M, c,d)  $24 \times 10^{-9}$  M, and e,f)  $58 \times 10^{-9}$  M. Histograms were plotted from the measurement of 200 nanoparticles.

nanoparticles compared to gold precursor leads to some homogeneous nucleation of gold particles. The high surface energy of gold nanoparticles causes coalescence to occur leading to agglomeration.<sup>[25]</sup> When the concentration was increased to  $24 \times 10^{-9}$  M, the nanoparticle size increased to  $160 \pm 20$  nm, corresponding to a 30 nm gold shell with an iron:gold ratio of 27:73 (Figure 2c; Figure S6, Supporting Information). Further increasing the concentration to  $58 \times 10^{-9}$  M resulted in nanoparticles  $140 \pm 20$  nm in size, corresponding to a 20 nm gold shell with an iron:gold ratio of 35:65 (Figure 2e; Figure S7, Supporting Information). Therefore,  $24 \times 10^{-9}$  and  $58 \times 10^{-9}$  M pre-gold seeded silica-coated magnetic nanoparticles are sufficiently low concentrations so as to enable a complete gold shell, but high enough to prevent the formation of aggregates.

To test the colloidal stability of the gold-coated magnetic, changes in hydrodynamic size and polydispersity index (PDI) versus time were recorded (Figure S5, Supporting Information). No sign of flocculation was observed up to 270 min with the PDI remaining stable. After 270 min, a sudden decrease in hydrodynamic size from 153 to 134 nm along with a reduction of the PDI from 0.134 to 0.117 suggest the few bigger particles may have deposited as sediment at the bottom of the vessel. Further measurements up to 750 min showed no significant changes in size or PDI hence, showing a stable dispersion of particles in solution.

The X-ray diffraction (XRD) patterns for the iron oxide, silica-coated, gold seeded, and gold-coated magnetic nanoparticles confirm that no change in the iron oxide crystal structure is observed after coating (Figure S8 and Table S1, Supporting Information). The peaks match with crystalline face-centered cubic gold and magnetite patterns.<sup>[25–28]</sup> High resolution TEM (HRTEM) further confirms a crystalline Au shell, with atoms arranged in a face-centered cubic structure and interatomic distances that could be matched to Au(111) planes (Figure S9, Supporting Information).

## 2.2. Magnetic and Optical Properties

The magnetic and optical properties of the particles were measured to investigate their applicability for magnetoplasmonic sensing. As shown in the magnetization ( $M$ ), applied field ( $H$ ) plot, the saturation magnetization decreases from 56 to 36  $\text{emu g}^{-1}$  upon addition of silica and to 25  $\text{emu g}^{-1}$  upon addition of gold layers to the iron oxide nanoparticles (Figure 3a). The superparamagnetic behavior is retained regardless of the coating, with the remnant magnetization of  $\approx 5 \text{ emu g}^{-1}$  and a coercivity of  $\approx 11 \text{ Oe}$  (Figure S10, Supporting Information). These are in agreement with previous work for magnetite nanoparticles and coated magnetite nanoparticles,<sup>[4,11,29]</sup> indicating that the flow-based synthesis is as effective as other solution methods in retaining magnetic properties after coating.

The plasmonic properties are altered when the thickness of the gold shell is tuned by using different concentrations of pre-gold seeded magnetic nanoparticles. Broad absorbance peaks in the ultraviolet–visible spectra (UV–vis) at 710 and 780 nm were observed for the particles which were prepared with the initial pre-gold seeded silica-coated magnetic nanoparticles concentration of  $24 \times 10^{-9}$  and  $58 \times 10^{-9}$  M, respectively (Figure 3b). This

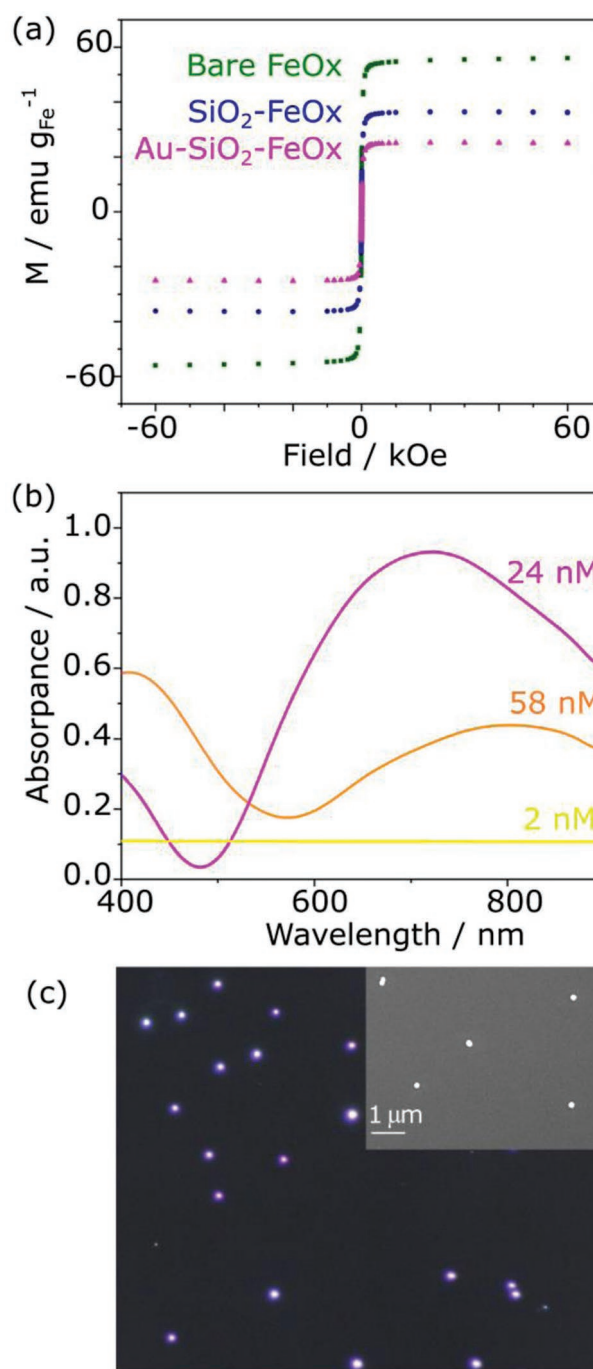


**Figure 3.** a) Superconducting quantum interference device (SQUID) magnetometry measured at 300 K of iron oxide nanoparticles (green) silica-coated magnetic nanoparticles (blue) and gold-coated magnetic nanoparticles (purple). b) UV–vis spectra of gold-coated magnetic nanoparticles with different initial pre-gold seeded silica-coated magnetic nanoparticles concentration  $2 \times 10^{-9}$  M (yellow),  $24 \times 10^{-9}$  M (orange), and  $58 \times 10^{-9}$  M (purple). c) Dark-field microscopy and SEM image (inset) of gold-coated magnetic nanoparticles prepared with  $24 \times 10^{-9}$  M seeded silica-coated magnetic nanoparticles.

is in agreement with the classical electromagnetic scattering theory, as by varying the thickness ratio of the dielectric core to the metallic shell optical resonance could be transferred to

any region of the optical spectrum.<sup>[30–32]</sup> As the particles are quite large, the broad spectrum is expected. The nanoparticles formed from  $2 \times 10^{-9}$  M solution showed no observable absorbance peak in the UV–vis spectrum due to the sedimentation as a result of the aggregation of the particles.

The optical properties of the gold-coated magnetic nanoparticles made with different concentrations of pre-gold seeded silica-coated magnetic nanoparticles were further investigated using dark-field microscopy and scanning electron microscopy (SEM) (Figure S11, Supporting Information). The nonaggregated gold-coated magnetic nanoparticles disperse evenly on a substrate (Figure 3c, inset) and create purple spots due to the scattering at precise locations (Figure 3c). The good dispersion and overall uniform shape and size of gold coated magnetic nanoparticles achieved by the flow-based method creates few variations in the optical signal, which is important for optical sensing applications.<sup>[33,34]</sup>

### 2.3. Biomolecular Sensing

To evaluate the effectiveness of the flow-based method for producing gold-coated magnetic nanoparticles for SERS applications, gold-coated magnetic nanoparticles were modified with Raman probe molecules. Thiol based (-SH) 4-mercaptobenzoic acid (4-MBA) was considered as the Raman active molecule to prepare the SERS particles.<sup>[35]</sup> The obtained SERS spectra from these SERS particles prepared from gold-coated magnetic nanoparticles is illustrated in Figure 4. Two distinct SERS bands are observed at 1076 and 1586  $\text{cm}^{-1}$  corresponding to the aromatic ring vibrations such as  $\nu_{12}$ -ring breathing and  $\nu_{8a}$ -ring breathing of 4-MBA. This was observed in the resultant SERS spectra which have a good agreement with the literature indicates the chemisorption of 4-MBA on gold-coated magnetic nanoparticles surface.<sup>[36–38]</sup> The SERS performance of these particles was validated by investigating the effect of concentration of 4-MBA molecules (arrow in Figure 4) where the enhancement of SERS

intensity was found with the increase in coverage of the Raman active molecules to the point where a full monolayer coverage was achieved.<sup>[39,40]</sup>

### 3. Conclusion

In conclusion, we have developed a rapid, flow-based synthetic method for producing gold-coated nanoparticles that match the quality of particles produced from slower, benchtop colloidal syntheses. The 2 and 3 syringe setup enables intimate mixing of reagents that form uniform gold seeds and then a complete gold shell around silica coated nanoparticles. The method reported here is simple, scalable, cost-effective, and fast. We show that the flow-based synthesis is effective for producing gold-coated magnetic nanoparticles with excellent optical and magnetic properties for use as magnetoplasmonic sensors. Because the gold coating occurs on silica encapsulated nanoparticles, the flow-based method is anticipated to enable plasmonic properties to be added to wide range of materials.

### 4. Experimental Section

**Materials:** Iron(III) acetylacetonate (97%), oleylamine (98%), oleic acid (90%), trioctylamine (98%), igepal CO-520, ammonium hydroxide (30%), tetraethylorthosilicate (TEOS), [3-(2-aminoethylamino) propyl] trimethoxysilane (80%) (AEAPTMS), (3-aminopropyl) triethoxysilane (APTES), dimethyl sulfoxide (DMSO), gold(III) chloride trihydrate ( $\text{HAuCl}_4 \cdot 3\text{H}_2\text{O}$ , 99.99% trace metals), tetramethylammonium hydroxide in methanol solution (25% (wt/vol) TMAOH in methanol solution), hydroxylamine hydrochloride ( $\text{NH}_2\text{OH} \cdot \text{HCl}$ ), sodium citrate dihydrate, sodium borohydride (99.99% trace metals), 4-MBA (99%) were purchased from Sigma-Aldrich. Acetone (reagent grade), toluene (reagent grade), cyclohexane (reagent grade), methanol (reagent grade), nitric acid (69%), and hydrochloric acid (32%) were purchased from Chem-Supply Australia. Polylactic acid was purchased from Flashforge. Except for oleylamine chemicals were used as received. oleylamine was distilled before reaction. Syringes were purchased from Terumo syringe, needles ( $0.7 \times 38$  mm) were purchased from BD. Glassware was cleaned with freshly prepared aqua regia ( $\text{HCl}:\text{HNO}_3$  in a 3:1 ratio by volume) followed by rinsing with a copious amount of Milli-Q water.

**Silica-Coated Magnetic Nanoparticles:** Magnetic iron oxide nanoparticles were synthesized by thermally decomposing iron(III) acetylacetonate (260 mg, 0.7 mol) in a solution of oleylamine (2.4 mL, 7 mmol), oleic acid (0.6 mL, 1.7 mmol), and trioctylamine (2.4 mL, 5.4 mmol) at the reflux temperature of 330 °C. A silica shell was formed around the iron oxide nanoparticles using a standard microemulsion sol-gel method involving the base-catalyzed hydrolysis and polycondensation of TEOS on the surface of magnetic nanoparticles.<sup>[11]</sup> 12 mL cyclohexane was added to a 40 mL vial and then igepal (700  $\mu\text{L}$ , average Mn 441) CO-520 was added. The solution was vortexed to dissolve the igepal CO-520 completely. A 100  $\mu\text{L}$  of the  $3 \times 10^{-6}$  M of iron oxide nanoparticles in toluene was added to the solution. Next ammonium hydroxide (85  $\mu\text{L}$ , 0.65 mmol) was added to the solution and the vial was shaken by hand for few seconds. Finally, TEOS (30  $\mu\text{L}$ , 0.13 mmol) was added to the solution and the vial was left inside a fume hood for 42 h. To terminate the surface of the silica-coated magnetic nanoparticles with amine group, AEAPTMS (7  $\mu\text{L}$ , 0.026 mmol) was added to the microemulsion solution of the silica-coated magnetic nanoparticles and shaken for 120 min. The microemulsion was broken by adding TMAOH (4 mL,  $50 \times 10^{-3}$  M in methanol) and then carefully collecting the brown layer from the solution. Then 8 mL acetone was added to the solution and the particles solution was transferred to

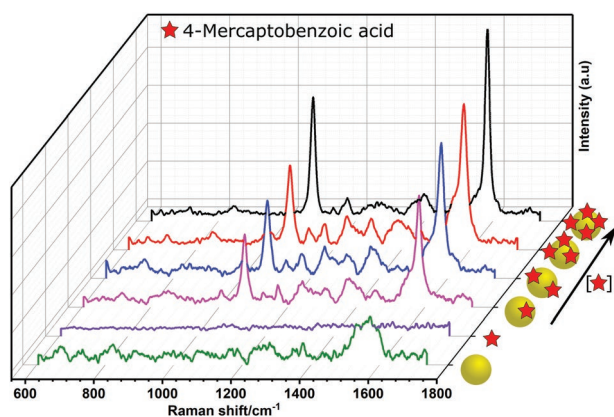


**Figure 4.** Raman spectra of bare gold-coated magnetic nanoparticles (green), 4-MBA Raman active molecule (purple), and SERS spectra of gold-coated magnetic nanoparticles modified with  $3 \times 10^{-6}$  M of 4-MBA (magenta), gold-coated magnetic nanoparticles modified with  $5 \times 10^{-6}$  M of 4-MBA (blue), gold-coated magnetic nanoparticles modified with  $20 \times 10^{-6}$  M of 4-MBA (red), and gold-coated magnetic nanoparticles modified with  $1 \times 10^{-3}$  M of 4-MBA (black).

the centrifuge tubes. Particles were centrifuged at 1600 rcf for 15 min then the supernatant was removed (this step was repeated twice). The acquired nanoparticles were redispersed in 1 mL DMSO sonicated and transferred to the centrifuge tube again. The particles were centrifuged at 3800 rcf for 5 min and the supernatant was collected. Particles that precipitated out of the solution from the centrifuge tubes were discarded.

**Gold-Seeded Silica Coated Magnetic Nanoparticles:** The silica-coated magnetic nanoparticles collected from purification (1 mL,  $400 \times 10^{-9}$  M) were transferred to a 10 mL syringe containing gold(III) chloride trihydrate in aqueous solution (9 mL,  $0.25 \times 10^{-9}$  M) and sodium citrate aqueous solution (2 mL, 0.17 M). The second syringe (volume 1.5 mL) was loaded with an aqueous solution of sodium borohydride (1 mL, 0.01 M). Nanoparticles and streams of reagents were dropped into a 40 mL vial. The seeded particles were separated from the solution and washed using a neodymium square block magnet.

**Gold-Shell Silica-Coated Magnetic Nanoparticles:** Different concentrations of the pre-gold seeded silica-coated magnetic nanoparticles were dispersed in Milli-Q water and then loaded into a 1.5 mL syringe (1 mL,  $2 \times 10^{-9}$ – $58 \times 10^{-9}$  M). A second syringe (volume 12 mL) was loaded with gold(III) chloride trihydrate in aqueous solution (6.6 mL,  $0.3 \times 10^{-3}$  M) and sodium citrate aqueous solution (3.6 mL,  $10.8 \times 10^{-3}$  M) and a third syringe (volume 5 mL) were loaded with the hydroxylamine hydrochloride aqueous solution (3 mL,  $40 \times 10^{-3}$  M). Nanoparticles at the end of a piece were collected inside a vial and then further washed with Milli-Q water via magnetic separation. The reaction could theoretically be continuous as long as the supply of the chemicals and nanoparticles are available. After adding any sets of syringes containing the chemicals and particles a new Y-shaped piece was used to avoid clogging.

**SERS Preparation:** The particles used for SERS were prepared by the immobilization of 4-MBA on the surface of gold-coated magnetic nanoparticles. Briefly 50  $\mu$ L gold-coated magnetic nanoparticles ( $6 \times 10^{12}$  particles mL<sup>-1</sup>) was mixed with 50  $\mu$ L of different concentrations of 4-MBA and the resulting mixture was incubated for 2 h with shaking at room temperature.

**Instruments and Characterization:** TEM images were acquired using a Phillips CM 200 microscope at an acceleration voltage of 200 kV. The TEM samples were prepared by drop-casting a diluted solution of the nanoparticles on a carbon-coated copper grid, this was followed by air drying at room temperature. An FEI Nova Nano SEM 450 was used for acquiring SEM images of the gold-coated magnetic nanoparticles in the range of 4–25 kV. Both TEM and SEM images were analyzed by ImageJ software. The magnetic properties were investigated by SQUID magnetometry on a Quantum Design MPMS XL magnetometer with an external magnetic field ranging from 60 000 Oe (6 T) to –60 000 Oe (–6 T) at 300 K. A Cary 60 single-beam UV–vis spectrophotometer was used to acquire the absorbance spectra of the nanoparticles in solution. The hydrodynamic size of the gold-coated magnetic nanoparticles in Milli-Q water was measured on a Zetasizer Nano ZS. The colloidal stability of the gold-coated magnetic nanoparticles was measured over time using Zetasizer Nano ZS.

To measure the concentration of iron oxide nanoparticles, silica-coated magnetic nanoparticles and gold-seeded silica-coated magnetic nanoparticles, a NanoSight NS300 instrument was used to perform nanoparticle tracking analysis. Olympus BX51 dark-field microscopy was used to acquire dark-field images of the gold-coated magnetic nanoparticles. To achieve this, the gold-coated magnetic nanoparticles were immobilized onto APTES modified coverslips and then coverslips were rinsed with Milli-Q water and dried under a stream of argon. The coverslip was mounted on the aluminum holder and imaged using an Olympus BX51 microscope. Raman spectra were measured using a Renishaw in Via confocal Raman microscope with excitation laser wavelengths of 785 nm and the diffraction grating of 1200 g mm<sup>-1</sup>. Raman measurements were recorded by applying the laser power of  $\approx 2.01$  mW, accumulation time of three and exposure time of 10 s. The average of three measurements was used to present in SERS data and all the spectra were calibrated to silicon peak located

at 520–521 cm<sup>-1</sup>. XRD was performed on an Empyrean 2 (Malvern Panalytical) X-ray diffractometer with Co K $\alpha$  (1.79 Å) radiation sample was analyzed from 30° to 100° (2 $\theta$ ).

## Supporting Information

Supporting Information is available from the Wiley Online Library or from the author.

## Acknowledgements

This work was financially supported by the Australian Research Council (LP150101014, J.J.G. and R.D.T.), the Australian Laureate Fellowship (FT150100060, J.J.G.), and the Discovery Project (DP190102659 and DP200100143, R.D.T.). J.J.G. also acknowledges a National Health and Medical Research Investigator grant (GNT1196648). L.G., J.J.G., and R.D.T. acknowledge the Dementia Australia Research Foundation Yulgilbar innovation grant.

Open access publishing facilitated by University of New South Wales, as part of the Wiley - University of New South Wales agreement via the Council of Australian University Librarians.

## Conflict of Interest

The authors declare no conflict of interest.

## Data Availability Statement

The data that support the findings of this study are available from the corresponding author upon reasonable request.

## Keywords

flow synthesis, gold-coated magnetic nanoparticles, gold coating, magnetic nanoparticles, magnetic sensing, optical sensing, plasmonic sensing

Received: March 16, 2022

Revised: April 29, 2022

Published online: June 17, 2022

- [1] R. Tavalalaie, J. Mccarroll, M. Le Grand, N. Ariotti, W. Schuhmann, E. Bakker, R. D. Tilley, D. B. Hibbert, M. Kavallaris, J. J. Gooding, *Nat. Nanotechnol.* **2018**, *13*, 1066.
- [2] H. Jahangirian, K. Kalantari, Z. Izadiyan, R. Rafiee-Moghaddam, K. Shamel, T. J. Webster, *Int. J. Nanomed.* **2019**, *14*, 1633.
- [3] L. Gloag, M. Mehdipour, D. Chen, R. D. Tilley, J. J. Gooding, *Adv. Mater.* **2019**, *31*, 1904385.
- [4] J. Wang, X. Wu, C. Wang, Z. Rong, H. Ding, H. Li, S. Li, N. Shao, P. Dong, R. Xiao, S. Wang, *ACS Appl. Mater. Interfaces* **2016**, *8*, 19958.
- [5] C. Caro, F. Gámez, P. Quaresma, J. M. Páez-Muñoz, A. Domínguez, J. R. Pearson, M. Pernía Leal, A. M. Beltrán, Y. Fernandez-Afonso, J. M. De la Fuente, R. Franco, E. Pereira, M. L. García-Martín, *Pharmaceutics* **2021**, *13*, 416.
- [6] A. Koudrina, C. Chartrand, G. O. Cron, J. O'Brien, E. C. Tsai, M. C. DeRosa, *Chem. Commun.* **2022**, *58*, 2870.

- [7] A. C. Bohórquez, M. Unni, S. Belsare, A. Chiu-Lam, L. Rice, C. Pampo, D. Siemann, C. Rinaldi, *Bioconjugate Chem.* **2018**, *29*, 2793.
- [8] M. Bilal, Y. Zhao, T. Rasheed, H. M. N. Iqbal, *Int. J. Biol. Macromol.* **2018**, *120*, 2530.
- [9] Y. Gao, Y. Zhou, R. Chandrawati, *ACS Appl. Nano Mater.* **2020**, *3*, 1.
- [10] M. Sriram, K. Zong, S. R. C. Vivekchand, J. Justin Gooding, *Sensors* **2015**, *15*, 25774.
- [11] M. Mehdipour, L. Gloag, D. T. Bennett, S. Hoque, R. Pardehkhorrām, P. Bakthavathsalam, V. R. Gonçalves, R. D. Tilley, J. J. Gooding, *J. Mater. Chem. C* **2021**, *9*, 1034.
- [12] E. A. Kwizera, E. Chaffin, Y. Wang, X. Huang, *RSC Adv.* **2017**, *7*, 17137.
- [13] S. Moraes Silva, R. Tavallaie, L. Sandiford, R. D. Tilley, J. J. Gooding, *Chem. Commun.* **2016**, *52*, 7528.
- [14] S. Moraes Silva, R. Tavallaie, M. Tanzirul Alam, K. Chuah, J. J. Gooding, *Electroanalysis* **2016**, *28*, 431.
- [15] X. Hou, X. Wang, R. Liu, H. Zhang, X. Liu, Y. Zhang, *RSC Adv.* **2017**, *7*, 18844.
- [16] A. R. Poerwoprajitno, L. Gloag, J. Watt, S. Cheong, X. Tan, H. Lei, H. A. Tahini, A. Henson, B. Subhash, N. M. Bedford, B. K. Miller, P. B. O'Mara, T. M. Benedetti, D. L. Huber, W. Zhang, S. C. Smith, J. J. Gooding, W. Schuhmann, R. D. Tilley, *Nat. Catal.* **2022**, *5*, 231.
- [17] H. J. Kwon, K. Shin, M. Soh, H. Chang, J. Kim, J. Lee, G. Ko, B. H. Kim, D. Kim, T. Hyeon, *Adv. Mater.* **2018**, *30*, 1704290.
- [18] L. Zou, B. Huang, X. Zheng, H. Pan, Q. Zhang, W. Xie, Z. Zhao, X. Li, *Mater. Chem. Phys.* **2022**, *276*, 125384.
- [19] L. Syam Sundar, S. Mesfin, E. Venkata Ramana, Z. Said, A. C. M. Sousa, *Therm. Sci. Eng. Prog.* **2021**, *21*, 100799.
- [20] S. Duraiswamy, S. A. Khan, *Nano Lett.* **2010**, *10*, 3757.
- [21] A. Yoko, Y. Tanaka, G. Seong, D. Hojo, T. Tomai, T. Adschiri, *J. Phys. Chem. C* **2020**, *124*, 4772.
- [22] D.-B. Crys, B. de Nijs, A. R. Salmon, J. Huang, W. Wang, W.-H. Chen, O. A. Scherman, J. J. Baumberg, *ACS Nano* **2020**, *14*, 8689.
- [23] X. Zhang, L. Guo, J. Luo, X. Zhao, T. Wang, Y. Li, Y. Fu, *ACS Appl. Mater. Interfaces* **2016**, *8*, 9889.
- [24] J. Feng, D. Xu, F. Yang, J. Chen, C. Wu, Y. Yin, *Angew. Chem., Int. Ed.* **2021**, *60*, 16958.
- [25] B. Ingham, T. H. Lim, C. J. Dotzler, A. Henning, M. F. Toney, R. D. Tilley, *Chem. Mater.* **2011**, *23*, 3312.
- [26] H. Yu, M. Chen, P. M. Rice, S. X. Wang, R. L. White, S. Sun, *Nano Lett.* **2005**, *5*, 379.
- [27] G. Song, M. Chen, Y. Zhang, L. Cui, H. Qu, X. Zheng, M. Wintermark, Z. Liu, J. Rao, *Nano Lett.* **2018**, *18*, 182.
- [28] E. C. Vreeland, J. Watt, G. B. Schober, B. G. Hance, M. J. Austin, A. D. Price, B. D. Fellows, T. C. Monson, N. S. Hudak, L. Maldonado-Camargo, A. C. Bohorquez, C. Rinaldi, D. L. Huber, *Chem. Mater.* **2015**, *27*, 6059.
- [29] L. Gloag, M. Mehdipour, M. Ulanova, K. Mariandry, M. A. Nichol, D. J. Hernández-Castillo, J. Gaudet, R. Qiao, J. Zhang, M. Nelson, B. Thierry, M. A. Alvarez-Lemus, T. T. Tan, J. J. Gooding, N. Braidry, P. S. Sachdev, R. D. Tilley, *Chem. Commun.* **2020**, *56*, 3504.
- [30] K. R. Ryu, J. W. Ha, *RSC Adv.* **2020**, *10*, 16827.
- [31] A. Bonyár, *Biosensors* **2021**, *11*, 527.
- [32] M. Smith, M. McKeague, M. C. DeRosa, *MethodsX* **2019**, *6*, 333.
- [33] E. Alzahrani, *J. Anal. Methods Chem.* **2020**, *2020*, 6026312.
- [34] X. Liu, J. Wang, J. Gou, C. Ji, G. Cui, *Nanoscale Res. Lett.* **2018**, *13*, 335.
- [35] R. Pardehkhorrām, S. Bonaccorsi, H. Zhu, V. R. Gonçalves, Y. Wu, J. Liu, N. A. Lee, R. D. Tilley, J. J. Gooding, *Chem. Commun.* **2019**, *55*, 7707.
- [36] A. Williams, K. J. Flynn, Z. Xia, P. R. Dunstan, *J. Raman Spectrosc.* **2016**, *47*, 819.
- [37] X.-H. Pham, E. Hahm, K.-H. Huynh, B. S. Son, H.-M. Kim, D. H. Jeong, B.-H. Jun, *Int. J. Mol. Sci.* **2019**, *20*, 4841.
- [38] J. E. Park, N. Yonet-Tanyeri, E. Vander Ende, A.-I. Henry, B. E. Perez White, M. Mrksich, R. P. Van Duyne, *Nano Lett.* **2019**, *19*, 6862.
- [39] Y. Wang, S. Schlücker, *Analyst* **2013**, *138*, 2224.
- [40] A. I. Pérez-Jiménez, D. Lyu, Z. Lu, G. Liu, B. Ren, *Chem. Sci.* **2020**, *11*, 4563.